SAND2020-3141J

Hyperfine structures and isotopic shifts of uranium transitions using tunable laser spectroscopy of laser ablation plumes

S. S. Harilal[1], C. M. Murzyn[2], M. C. Phillips[3,4], and J. B. Martin[2]

[1]*Pacific Northwest National Laboratory, Richland, WA 99352, USA*
[2]*Sandia National Laboratories, Albuquerque, NM 87185, USA*
[3]*College of Optical Sciences, University of Arizona, Tucson, AZ 85721, USA*
[4]*Opticslah, LLC, Albuquerque, NM 87106, USA*

We report isotopic shifts and hyperfine structures of selected U transitions employing tunable spectroscopy *viz:* laser-induced fluorescence and laser absorption spectroscopy of laser ablation plumes. The plasmas were produced during ns laser ablation on a natural U metal target which contains 0.73% ^{235}U. Our results show that isotopic shifts between ^{238}U and ^{235}U are entangled with hyperfine structures of ^{235}U. The isotopic ratio obtained using laser-induced fluorescence is affected by the plasma reabsorption. Time-resolved laser absorption spectroscopy is carried out for evaluating the optical absorption and estimating the hyperfine constants.

Keywords: Laser ablation, Laser-induced fluorescence, Laser absorption spectroscopy, LIBS, Tunable laser spectroscopy, Isotopic analysis, Hyperfine structure, Uranium

1. Introduction

Optical spectroscopy in conjunction with laser-produced plasma (LPP) is a very promising tool for in-field and non-contact isotopic analysis of solid materials [1]. Both emission and absorbance/fluorescence spectroscopy of laser ablation plumes can be used for isotopic analysis. However, the reported isotopic shifts of U I and U II transitions in the visible spectral regime are in the range ~ 1-25 pm which necessitates the requirement of an extremely high-resolution spectrograph with a resolution ⩾ 60000 for using emission-based diagnostic tools (eg. laser-induced breakdown spectroscopy [1-3]) for isotopic analysis. In addition to this, the emission spectral analysis requires thermal excitation by electrons which happens at early times of plasma evolution when the lines are broader due to various line broadening mechanisms (Stark, Doppler etc.). Laser-absorption spectroscopy (LAS) and laser-induced fluorescence (LIF) tools can be used to marginalize the effect of instrumental broadening [1]. LAS and LIF probe the ground state atoms existing in the plasma when it is cooler, which inherently provides narrower lineshapes [4-9]. The reported linewidths of U transitions using LAS/LIF of laser-produced plasmas are ~ 1 pm which is significantly lower than the average isotopic shift of U atoms/ions (~ 9 pm) [10]. Recently several groups explored resonance excitation of LIBS plumes specifically for boosting the emission signal [11-14].

In addition to isotopic splitting, the hyperfine structures (hfs) may influence the lineshape of a transition. Hyperfine splitting is usually small; however, in certain cases, they can be larger than the isotope splitting. In that scenario, isotope shifts of atoms and molecules can be entangled with hyperfine structure. In addition to these, the high angular momentum and nuclear spin for ^{235}U (I = 7/2) leads to many hyperfine levels. Hyperfine structures of atomic transitions are routinely observed using high-resolution laser spectroscopy with cooled atomic reservoirs or atomic beams [15-18]. Several reports exist in the literature on isotopic and hyperfine analysis using LAS of LPP [1, 7, 19-22]. Here we report the hyperfine structures of ^{235}U using LIF of laser-ablation plumes. The results show that even in the relatively high-temperature laser-induced plasma environment, the ^{235}U hyperfine structure is observed. Our results show that the presence of optical saturation or reabsorption of emitted light in the LIF signal may influence the measured peak shapes and isotopic ratios. We used time-resolved LAS measurement for elucidating reabsorption effects seen in the LIF signal. The recorded hyperfine structures are also used for estimating the hfs constants.

2. Experimental Setup

A schematic of the experimental setup used in the present study is given in Fig. 1. The plasma plumes were generated by focusing 1064 nm, 6 ns full-width half maximum (FWHM) pulses from an Nd: YAG laser (Continuum, Surelite) with a spot size of ~1 mm. The laser energy and fluence at the target surface were ~48 mJ and ~ 6 J/cm^2 respectively. The target used was natural uranium, containing ~ 0.73% ^{235}U and ~ 99.27% ^{238}U, which was positioned in a chamber with a 10 Torr nitrogen ambient gas during measurements. The chamber was positioned on an x-y

translator so that the ablation spot can be changed for avoiding target drilling. A continuous-wave (cw) tunable Titanium-Sapphire laser (M-squared laser, SolsTiS) with a linewidth of ~50 kHz was used for LIF/LAS excitation with a mode-hop free scanning range of ~ 30 GHz. A wavemeter was used to monitor the probe laser wavelength. The cw probe pumping provides continuous excitation of the ground state atoms during the entire duration of the LPP lifetime [23]. The laser can be tuned in the wavelength range 700-990 nm and is also equipped with a resonant cavity frequency doubler. A collinear excitation scheme was used for LIF measurements where both the plasma producing and the LIF excitation beams approach the sample at a small angle. The LIF laser beam size at the target surface was ~ 4 mm in diameter and was overfilling the entire plasma plume volume. The LIF probe laser was scanned over 30 GHz of spectral range for recording the excitation spectrum of selected transition. The LIF emission from the plasma was collected using a fiber positioned at near-normal angle with respect to the target surface and coupled to a 0.5 m Czerny-Turner spectrograph with 2400 grooves/mm grating (resolution ~ 40 pm). An intensified CCD (ICCD) was used for collecting the dispersed light. The spectrograph-ICCD combination was used for recording the 2D-fluorescence spectroscopy (2DFS) images [7, 10] which provided simultaneous absorption and emission spectral features. The spectral resolution available for LIF measurement is governed by the linewidth of the excitation laser beam and the various line broadening mechanisms present in a laser-produced plasma system. Instead, the available spectral resolution for an emission spectroscopic instrumentation is dictated by the spectrograph resolution. The LIF measurement was carried out by collecting light from the entire plume (spatially integrated) and by averaging over two shots.

For performing LAS, a part of the probe beam with ~ 1 mm diameter was directed through the ablation plume at a distance ~ 0.5 mm from the target. After passing through the plasma plume, the probe was directed through a 1" right-angled prism to a Si photodiode with 200 ns rise time. The prism provided spectral filtering of the probe laser from the plasma emission. The photodiode signal was digitized at 1 MHz using a data acquisition (DAQ) board. For measuring the absorption spectra, the wavelength of the probe laser was scanned and the time-resolved transmission profile was recorded for each laser shot. The LAS signal collection and the scanning of the cw laser were controlled by a LabVIEW program. The probe transmission I(f,t) was converted to absorbance using the equation:

$$A(f,t) = -\ln[I(f,t)/I_o(f)] \qquad (1)$$

where $I_0(f)$ is the transmitted signal before ablation event. The acquired time-resolved data was converted into 2D maps of time-resolved absorbance vs frequency.

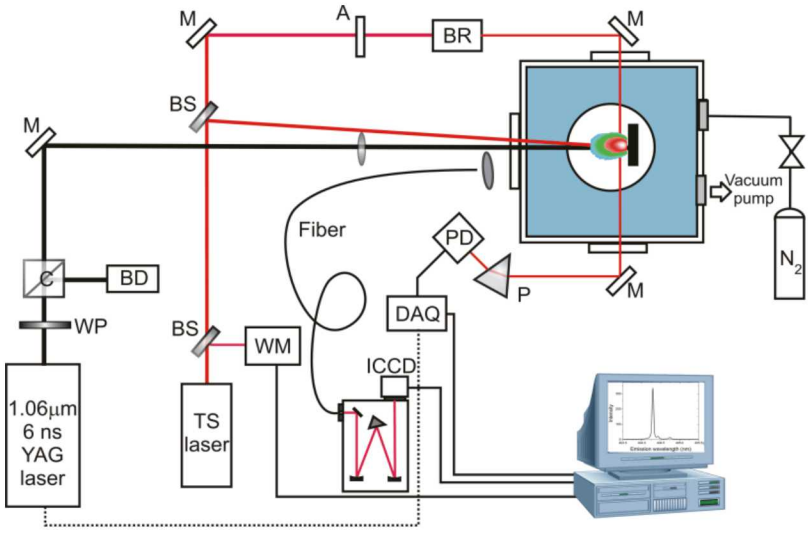

Figure 1: Schematic of the experimental setup. A Nd:YAG laser was used for ablation. For LIF/LAS probing, a tunable cw Ti:Sapphire laser was used. (WM, wavemeter; PD, photodiode; DAQ, data acquisition board; BD, beam dump; WP, waveplate; C, cube polarizer; M, mirror, A, attenuator; BR, beam reducer, P, prism).

3. Results and Discussion

Uranium emission features are very congested. For example, there exist ~ 92000 U I and U II transitions that originated from ~1600 energy levels in the ultraviolet-visible spectral region [1, 24]. Hence resolving uranium transitions in the UV-VIS spectral region requires high-resolution spectroscopic tools. Both LIF and LAS probe ground state populations of the selected transition and offer a high spectral resolution which is defined by the bandwidth of the probe beam. In LAS, the absorption of the probe beam is monitored. In LIF, the emission resulting from the decay of the resonantly excited atoms is monitored. However, scattering of the light may be an issue if the LIF emission wavelength is similar to the probe wavelength considering cw laser is used for resonant excitation in the present experiment. The scattering issue can be avoided by monitoring the relaxation of the excited atoms to other energy levels coupled to the resonantly pumped upper energy level. For U, numerous transitions share the same upper energy level. Since the LIF technique combines both the absorption and emission processes, the line selection for isotopic analysis is also very important. For obtaining the highest signal to noise ratios, the lines (both excitation and emission) with higher gf values where g is the term value and f is the oscillator strength of the selected atomic transition. But reabsorption of the LIF emitted photons may occur if the selected lines are having high gf. In addition to these, the isotopic shifts of selected lines should be greater than the linewidths of the transitions in the plasma plume.

The selected transitions for the present study includes (i) U I absorption at 763.385 nm (3801 cm^{-1}-16900 cm^{-1}, gf = 0.049), isotopic splitting (IS) ~ 17.2 pm, direct-line fluorescence at U I 591.70 nm (0 cm^{-1}-16900 cm^{-1}, gf

=0.185); (ii) U I absorption at 713.087 nm (620 cm^{-1}-14,644 cm^{-1}, gf = 0.067), IS ~19.8 pm, emission at 682.8 nm (0 cm^{-1}-14644 cm^{-1}, gf = 0.12). Figs. 2(a) and 3(a) give 2DFS, which combine emission and absorption of selected transitions. For obtaining 2DFS, the LIF laser was stepped across the selected U transition and the emission from the coupled transition is monitored. The pump beam scattered light is avoided by selecting transitions whose fluorescence and excitation wavelengths are far apart. The excitation spectra and partial energy level diagrams of selected transitions are given in Figs. 2b and 3b. The measurements were carried out at a chamber pressure of 10 Torr N_2 with delay and gating times of 50 μs and 150 μs respectively.

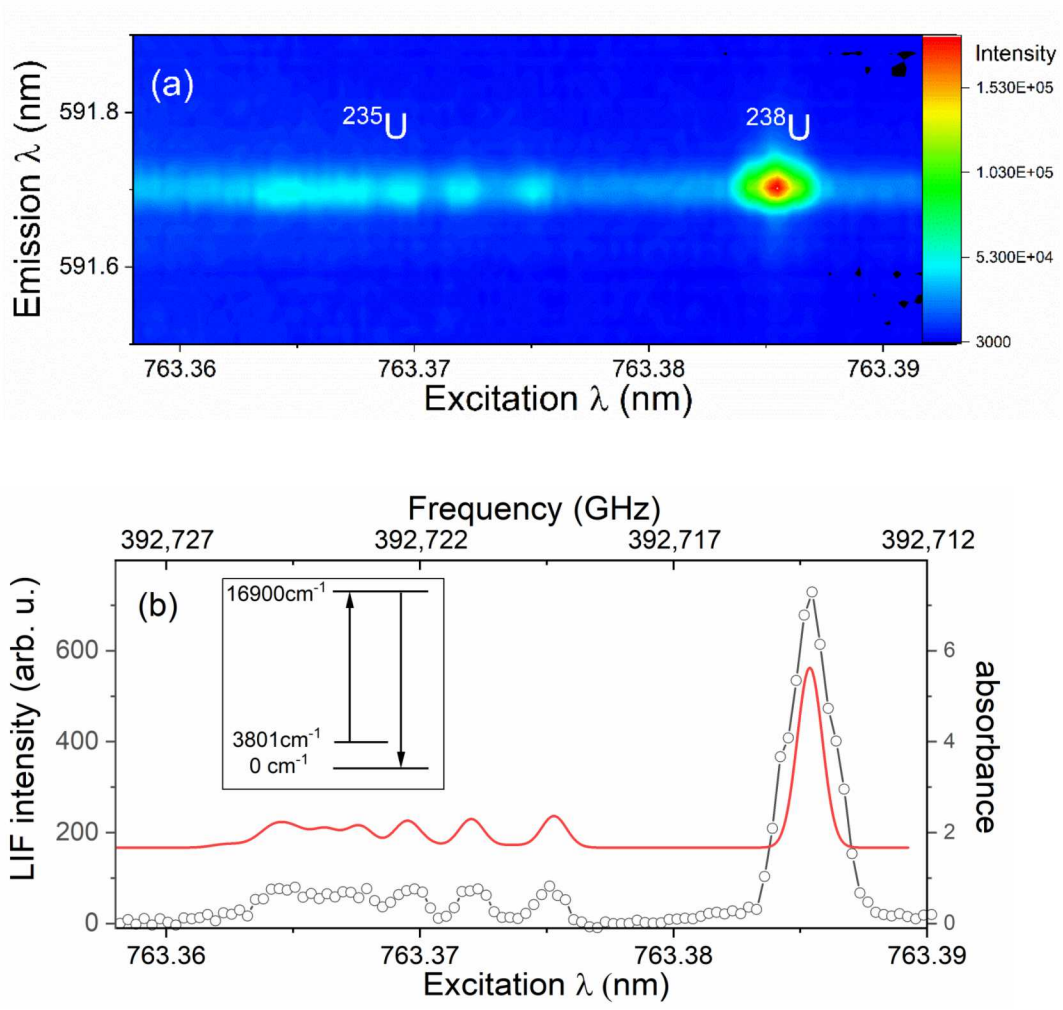

Figure 2: (a) The 2DFS of U transition at 763.385 nm and (b) the excitation spectrum obtained from 2DFS (bottom, black). The wavelengths given (excitation and emission) correspond to the vacuum wavelength. The partial energy levels of selected transitions are given in the inset. The red curve is a modeled hfs spectrum.

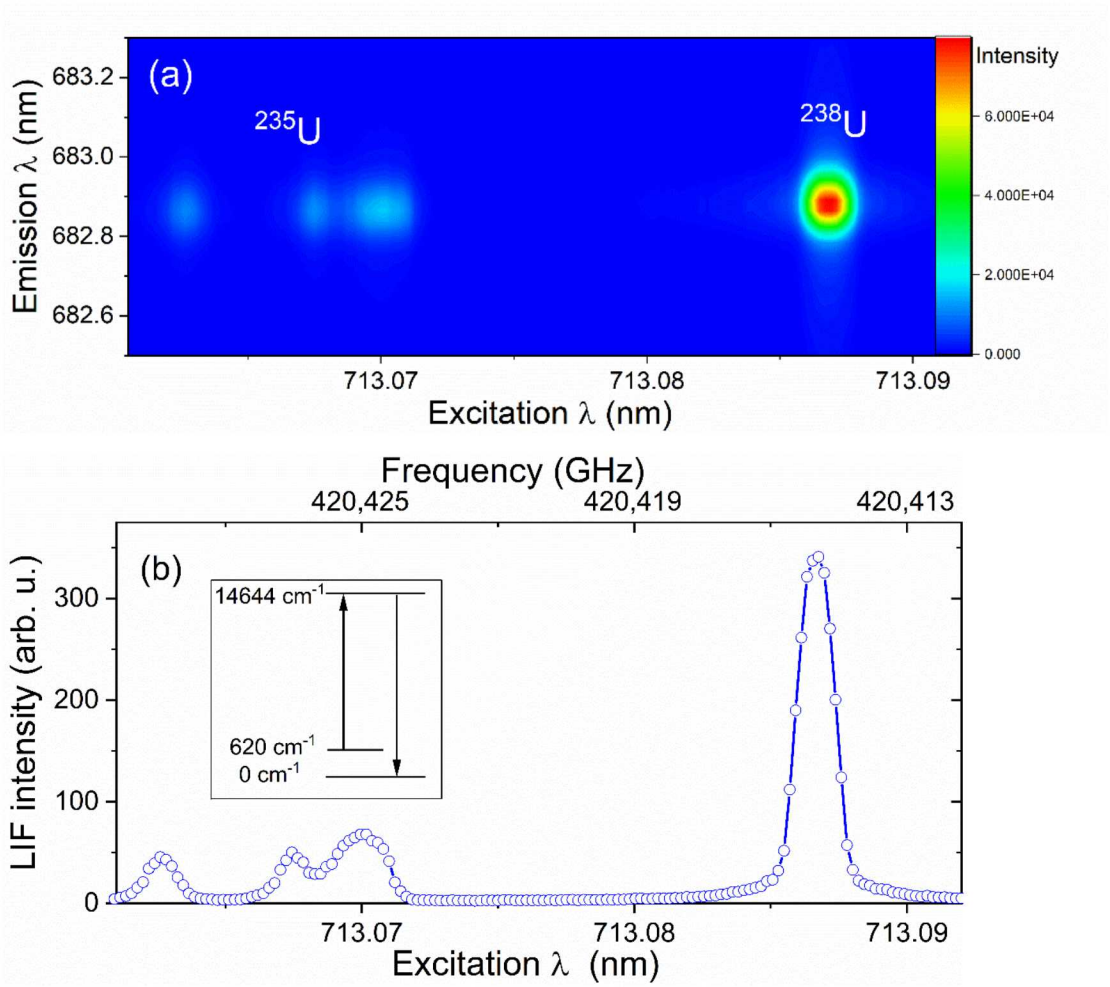

Figure 3: (a) The 2DFS of U transition at 713.087 nm and (b) the excitation spectra obtained from 2DFS. The wavelengths given (excitation and emission) correspond to the vacuum wavelength. The partial energy levels of selected transitions are given in the inset.

The 2DFS images show strong emission from ^{238}U in comparison with ^{235}U emission which is consistent with low-concentration ^{235}U in the natural U sample. The 2DFS and the excitation spectra clearly show isotopic shifts between ^{235}U and ^{238}U as well as the hfs of ^{235}U. The isotopic shifts of U I transitions at 713.087 nm and 763.385 are ~19.8 pm and ~17.2 pm respectively which agree well with measured shifts. However, the excitation spectra given in Figs. 2 and 3 show the isotopic shifts are entangled with hyperfine structures of ^{235}U. For nuclei with an even atomic number and even mass number, the spin angular momentum is zero and hence no hfs is observed in ^{238}U spectral lines. Because of the presence of the hfs, the ^{235}U exhibits a broadened spectrum with fine structures in comparison with the ^{238}U spectrum.

A modeled HFS absorption spectrum is also given in Figure 2b. Hyperfine structures for the ^{235}U I 763.385 nm was calculated using data available in the literature [25, 26] and a modeled absorption spectrum using the allowed 22 hyperfine transitions with each hyperfine transition modeled as a Gaussian width of 0.6 GHz FWHM. The experimentally recorded hfs agrees well with the modeled spectrum. The modeling of the absorption spectrum of ^{235}U I 713.087 nm is discussed later in the paper. According to the Figs. 2 and 3, the LIF signal intensity from ^{235}U is very significant even though the sample contains trace amounts of ^{235}U (0.73% by wt.). It highlights the sensitivity of the LIF technique for identifying samples even with very low enrichment. The opacity effects of the plasma may influence both the absorption and emission and the distortion seen in the lineshapes of the ^{238}U peak can be related to plasma opacity effects. The decoupling of these two processes (absorption and emission) will be a challenging task with the present LIF experimental scheme considering the time-integrated measurement as well as the cw collinear LIF excitation scheme. The collinear geometry will be useful for standoff detection [27] and the LIF beam illuminates the entire plasma volume. Considering the large space-time gradients in temperature and density of laser-produced plasma [1], time and space resolved studies are essential to tackle reabsorption effects. Time-resolved LAS measurement will be helpful to understand the plasma reabsorption effects seen in the 2D-LIF measurements.

To investigate the time-dependence of the plasma with spatial precision, the time-resolved absorption spectroscopy (TRAS) measurements were carried out. Figure 4 gives the TRAS map and LAS spectra of the U I absorbance at 713.087 nm, as a function of time after ablation. The absorption of both transitions from U isotopes follows the same general behavior, with an initial rise in absorption peak height followed by a slower decay. The absorption map is also consistent with 2DFS given in Figure 3. The ^{238}U absorption is stronger as expected, primarily due to the higher atomic number density of ^{238}U (99.3%) relative to ^{235}U in the plume. However, the weaker ^{235}U absorption is visible for $\geq$ 300 μs after ablation before decreasing below measurement noise levels.

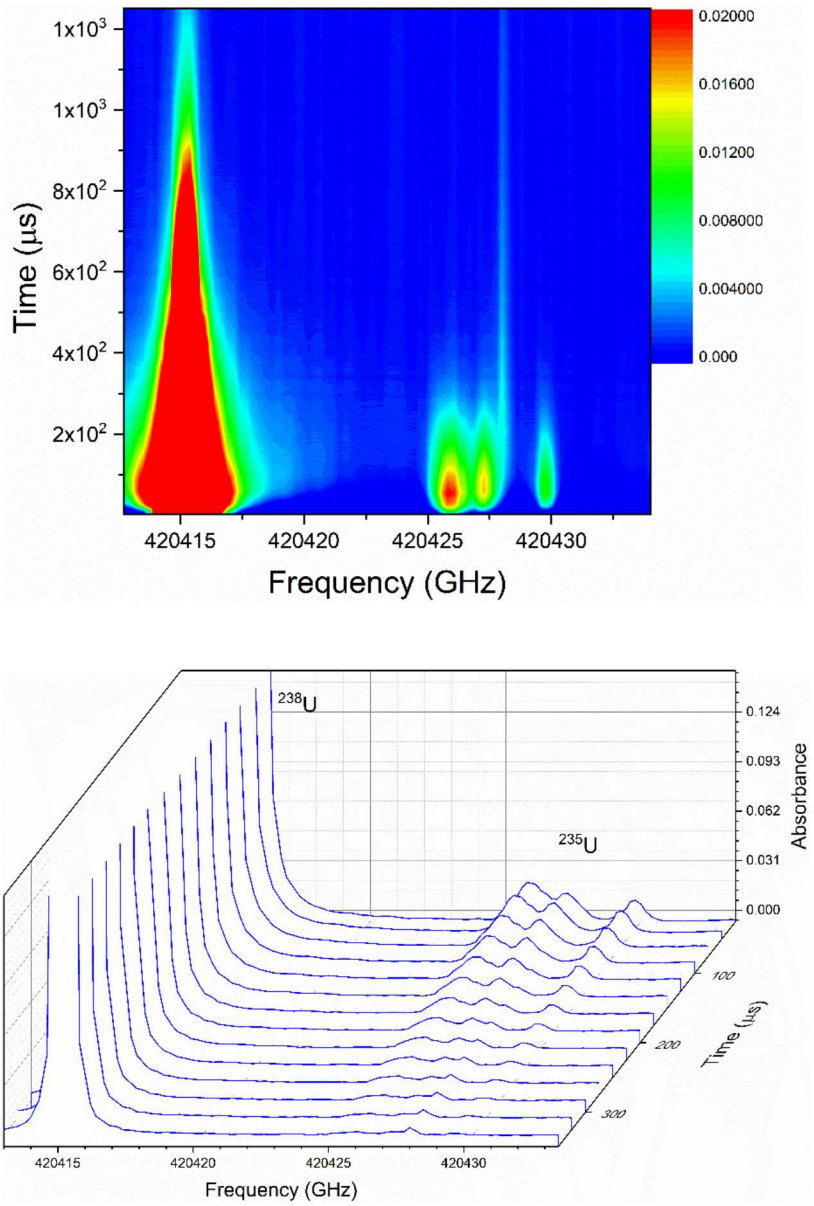

Figure 4: TRAS map of the U I 713.087 nm absorbance is given (top) as a function of time after ablation. LAS spectra at various times after the ablation onset are given (bottom).

One significant difference between the 2DFS and TRAS measurements is the excitation beam geometry. Unlike LIF beam, which excites the entire plume from the collinear direction, the LAS probe beam with a diameter 1 mm was directed through the ablation plume, parallel to the sample at a distance of ~500 µm above the surface. It should be mentioned that the measured absorbance is integrated along the probe propagation path through the plume. However, even though the line of slight averaging will be present in TRAS results, it still provides significantly higher spatial precision compared 2DFS. In addition to these, the LIF measurement is carried out in a time-integrated manner and a predictive understanding of the LIF signal-generation process in the complex LPP environments is lacking. LIF

signal levels are also very sensitive to quenching effects (collisional energy transfer) rates which may vary with local conditions in the plasma plume. Furthermore, the plasma reabsorption effects during emission may cause signal saturation. The time-resolved LAS signal given in Figure 4 clearly shows the time dependence of the bulk and trace isotopes. The ^{238}U signal is observed for times ≥ 1 ms while the ^{235}U is detected above the noise floor only at early times (up to ~ 300 μs) of plasma evolution due to the lower number density of the minor isotope. TRAS map given in Figure 4 shows the presence of a delayed, narrow linewidth and persistent resonant absorption feature at ~ 420428 GHz and it is not assigned.

Although hfs constants for the ^{235}U transition originating from 14,644 cm^{-1} energy level are available in the literature [28, 29], it showed significant differences with respect to hfs structures measured in the present studies. Hence a physically resolved model was fit to the LAS data in order to empirically estimate the hyperfine constants (A/B) for the 14,644 cm^{-1} energy level in ^{235}U. The absolute precision of hyperfine constants is lower than can be measured with other techniques, however, a model fit to the congested hfs structure is able to provide a first-order estimate to these parameters sufficient for many applications. Spectral modeling followed standard procedures for hyperfine splitting in atomic spectra that can be found elsewhere. To summarize, each fine energy level defined by J, is split into $(2J+1)$ hyperfine levels defined by the F quantum number ranging from: $F = J + I, J + I - 1, \ldots, |J - I|$. The energy shift in hyperfine levels relative to the fine structure was calculated with Casimir's formula [30]

$$\Delta E = \frac{1}{2}AK + \frac{B}{4}\frac{\frac{3}{2}K(K+1) - 2I(I+1)J(J+1)}{I(2I-1)J(2J-1)} \qquad (2)$$

where $K = F(F+1) - J(J+1) - I(I+1)$, A and B are the magnetic dipole and electric quadrupole hyperfine coefficients respectively. J is the total angular momentum of the energy level and I is the spin of the nucleus. The line strength distribution amongst hyperfine components in the electronic dipole transition was calculated as [31]

$$S_{FF'} = (2F+1)(2F'+1)\begin{Bmatrix} F & F' & 1 \\ J' & J & I \end{Bmatrix}^2 S_{JJ'} \qquad (3)$$

The term in curly brackets is the well-known Wigner-6j coefficient. Various authors have published this term with different ordering of the arguments, however the symmetry properties of the 6j coefficient make the calculation invariant under certain row and column operations. The 6j term also enforces the $\Delta F = 0, \pm 1$ selection rule. It should also be noted that when calculating hyperfine line strengths as presented here it is important to account for the (2I+1) nuclear degeneracy so as to satisfy the normalization condition. Applying these equations to the LAS model, the energy levels coupling to give the 713.087nm in ^{238}U (14,643.867cm^{-1}, 620.323 cm^{-1}) were obtained from the

venerable Blaise compilation [17]. The 14,644cm^{-1} level was corrected for its 238-235 isotopic mass and field shift (-0.380cm^{-1}) [17]. The 620 cm^{-1} energy level has no shift.

The hyperfine coefficients for the metastable 620 cm^{-1} level were taken from Childs et. al. (A: -68.3457 MHz, B: 40.110 MHz) [32]. The hyperfine parameters for the 14,644 cm^{-1} level were left as free parameters for fitting to the data using a Nelder-Mead optimization function. The relative intensity distribution amongst the hyperfine components was calculated and then each transition dressed in a properly normalized Voigt function with 0.022 cm^{-1} (0.66 GHz) Doppler and 0.0035cm^{-1} (0.10 GHz) Lorentz components. These parameters were estimated by approximating the lineshape observed in the isolated hyperfine component F'-F = 9.5-8.5. The wings of the ^{238}U line were fit independently to account for resonant absorption in the Lorentz wings.

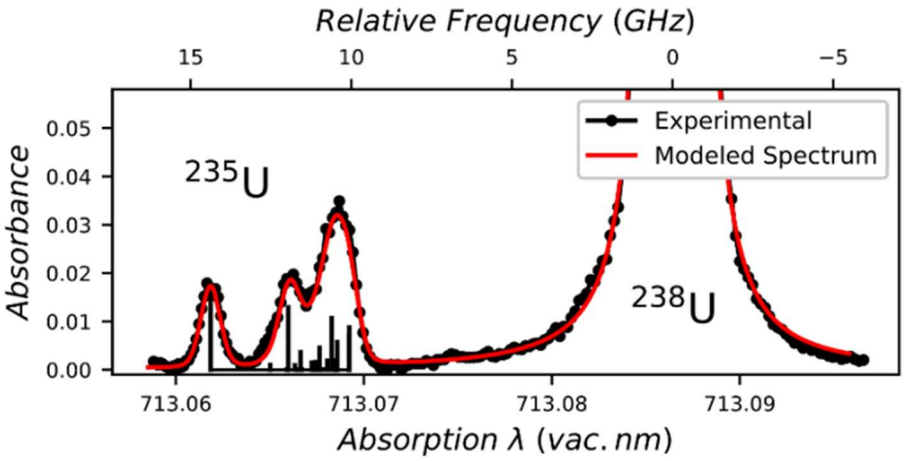

Figure 5: Experimental LAS spectrum from 66 μs after ablation with the model fit to the overlapping hyperfine ^{235}U and fine ^{238}U transitions. Stick plot beneath the hyperfine structure represents the relative intensity of the 21 hyperfine transitions contributing to the observed structure in the hfs spectrum.

It was found that the model was readily able to reproduce the width and intensity pattern of the hyperfine manifold measured in the LAS data. The resulting spectral model shown in Figure 5 was fit with A: 20.1 MHz and B: 4,949.7 MHz for the 14,644cm^{-1} energy level of ^{235}U. These hfs constants differ significantly from the values reported in the literature [28, 29] for this level. To assess the validity of using a model regression to estimate the A/B coefficients of the 14,644 cm^{-1} level, a numerical analysis was conducted over the 2-dimensional solution space. An analysis of ±10,000 MHz for both coefficients was conducted. A reduced scope of that analysis is shown in Figure 6. Not surprisingly, the results for such a highly nonlinear problem depict a residual surface with many local minima potentially making gradient-based optimization sensitive to initial guesses. The analysis does, however, show a global minimum (optimal fit) corresponding to the A/B coefficients that were arrived at with the Nelder-Mead method. By

varying the subjective parameters used in fitting, we estimate the upper-bound of uncertainty in the A and B coefficients we report for the 14,644 cm^{-1} level to be ±3 MHz and ±120 MHz respectively. It should be noted that this approach remains very sensitive to the accuracy of the isotopic shifts and is likely not feasible in the case of all spectral lines.

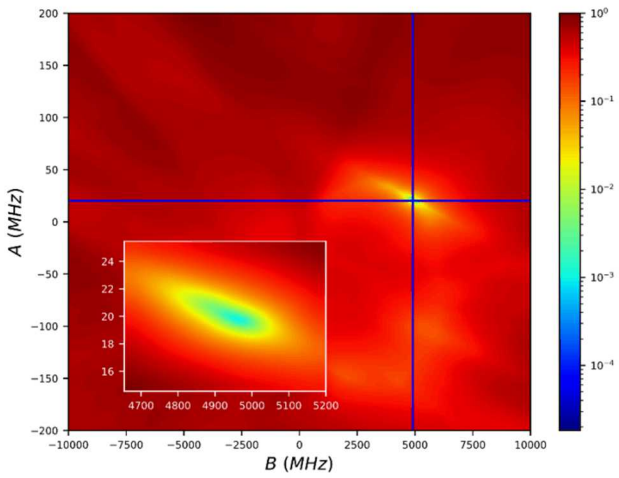

Figure 6: Normalized residuals for the HFS model regression in the 2-dimensional (A/B) solution space of the 713.087 nm LAS spectrum. The global minimum is shown with blue crosshairs. The inset figure shows a bicubic interpolation of calculated points around the global minimum.

The ratio of absorption peak areas between ^{235}U (summed over all hyperfine transitions) and ^{238}U provides the isotope ratio, assuming the peak areas are measured accurately. In particular, plasma reabsorption effects in LIF and high optical density in LAS may lead to errors in measurement of the major isotope peak area. The ratio of peak areas measured with LIF shown in Fig. 2 and Fig. 3 is clearly not representative of the ratio R[$^{235}U/^{238}U$] = 0.73% expected for natural uranium. The ratio of peak areas measured with LAS in Fig. 4 and Fig. 5 appears closer to the expected value, but the high absorbance of the ^{238}U peak at early times makes accurate measurement of the peak area difficult. Our calculations showed that at early times, the ratio of peak areas is higher than 0.73%. At later times in the plasma, the ^{238}U peak becomes smaller and the estimation of its area becomes more accurate; as a result, the ratio of peak areas approaches the value of 0.7% at ~250 μs as expected for NU. However, the decreasing area of the ^{235}U peaks limits the ability to use later times in the plasma before they become undetectable above the noise.

The LIF emission signal is generated from the energy absorbed from the LIF excitation laser. Based on Eqn. (3) in Ref. [34], the detected LIF signal $S_F(\lambda_{ex}, t)$ can be expressed in a simplified form as:

$$S_F(\lambda_{ex}, t) = S_0 \cdot I_0 \cdot \left[1 - e^{-A(\lambda_{ex}, t)}\right] \quad (4)$$

where λ_{ex} is the wavelength of the laser exciting the LIF transition, t is time, S_0 is a constant factor incorporating collection area/efficiency and fluorescence quantum yield, I_0 is the incident laser intensity, and $A(\lambda_{ex}, t)$ is the absorbance experienced by the laser. For a simplified case of a spatially-uniform plasma with length L, the absorbance is given by $A(\lambda_{ex}, t) = \sigma_{12}(\lambda_{ex}) \cdot N_1(t) \cdot L$, where $\sigma_{12}(\lambda_{ex})$ is the absorption cross-section, $N_1(t)$ is the atomic population in the lower state pumped by the LIF excitation laser. Eqn. (1) is linear in the incident laser intensity I_0 and thus ignores optical saturation or optical pumping effects arising at high laser intensities, which is more common with pulsed LIF than with the CW LIF used in our experiments. Eqn. (4) also ignores any reabsorption of the LIF emission. For $A(\lambda_{ex}, t) \ll 1$, Eqn. (1) simplifies to $S_F(\lambda_{ex}, t) \sim S_0 \cdot I_0 \cdot [\sigma_{12}(\lambda_{ex}) \cdot N_1(t) \cdot L]$ and under these conditions of low optical density, the LIF signal is linear with atomic number density. Under conditions of very high optical density $A(\lambda_{ex}, t) \gg 1$, Eqn. (4) approaches a constant value $S_F(\lambda_{ex}, t) \sim S_0 \cdot I_0$ corresponding to complete absorption of the incident laser after which the LIF signal cannot increase further. Thus, under conditions of high optical density, the LIF intensity is nonlinear with the atomic number density and approaches a maximum value. Correspondingly, because the absorbance depends on the excitation wavelength, the lineshape of the LIF excitation spectrum deviates from the absorbance spectrum lineshape $\sigma_{12}(\lambda_{ex})$.

The results in Fig. 4 verify that the ^{235}U absorbance is low (< 0.03) throughout the plasma evolution. Thus, it is reasonable to assume the LIF excitation spectra are linear in ^{235}U number density and the LIF excitation spectra are proportional to the absorbance spectra. In contrast, the ^{238}U absorbance is high (>0.1 most times and >1 in many cases) near the line center which leads to the distorted LIF excitation spectra observed in Fig. 2 and Fig. 3. It is also noted that the absorbance spectrum may also become distorted in the presence of high optical density, leading to nonlinearity between the area under the absorbance peak and the atomic number density. Besides, it can be difficult to measure high absorbances accurately given the high dynamic range required to measure both the low transmitted light and the high incident intensity.

Figure 7(a) and Fig. 8(a) show simulated absorbance spectra for the U I 713.087 nm and the U I 763.385 nm transitions, respectively, including the modeled hyperfine structure. Individual peaks were modeled by Voigt profiles with 660 MHz Gaussian FWHM and 100 MHz Lorentzian FWHM. The areas of the ^{235}U and ^{238}U peaks are scaled to represent natural U with 0.73% ^{235}U. In absorbance, the peak areas are assumed to be linear with atomic number density over the range plotted. Figure 7(b) and Fig. 8(b) show simulated LIF excitation spectra modeled using Eqn. (1) based on the absorbance spectra shown in Fig. 7(a) and Fig. 8(a), respectively. The lower blue curves show the modeled LIF signal for the absorbance as plotted in (a), and the upper red curves show the modeled LIF signal with the absorbance spectra multiplied by 10. The high absorbance near the ^{238}U peaks leads to a highly nonlinear dependence of LIF emission intensity on absorbance. The net effect of the nonlinearity is an apparent increase in height of the ^{235}U peaks relative to the ^{238}U peaks in the LIF excitation spectrum. Qualitatively similar effects on the relative peak areas of ^{235}U and ^{238}U were observed in Fig. 2 and Fig. 3, which we attribute primarily to the high absorbance of the ^{238}U peak, as verified by the TRAS results shown in Fig. 4. Besides, other nonlinearities in the LIF

emission signal due to optical saturation or reabsorption of emitted light may be present, leading to additional deviations of peak shapes and/or relative heights of ^{235}U versus ^{238}U peaks measured in the experimental LIF spectra.

In general, while LIF provides high sensitivity for trace element detection, it is challenging to use LIF for quantitative measurements of bulk elements due to the inherent nonlinearity of LIF signal with atomic number density under conditions of high absorbance. The same challenges exist for isotope ratio measurements when the isotopic abundances differ by large amounts. Possible solutions to improve quantification of isotope ratios using LIF include measuring different lines for major and minor isotopes to equalize the absorbance, although temperature-dependence of the line strengths must also be considered. Similar approaches are used with laser absorption spectroscopy for the detection of molecular isotopologues [35].

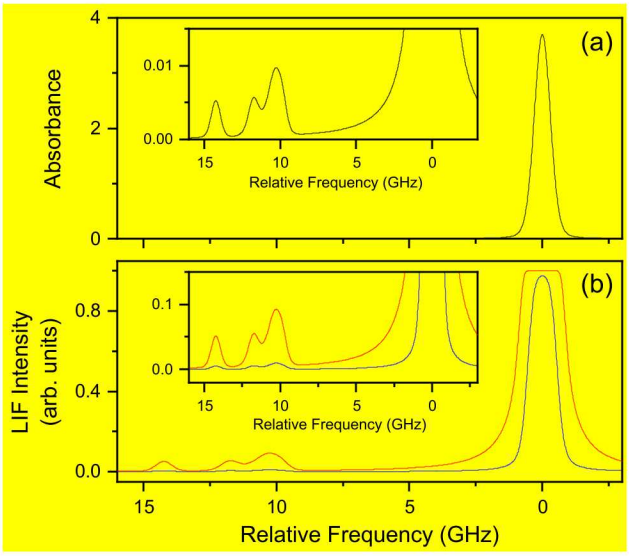

Figure 7. Simulated absorption and LIF spectra for U I 713.087 nm transition. (a) Absorbance spectrum with 0.7% ^{235}U. (b) LIF intensity spectrum calculated from the absorbance spectrum (blue, lower) and 10× absorbance spectrum (red, upper). Insets have re-scaled y-axis to show ^{235}U hyperfine structure.

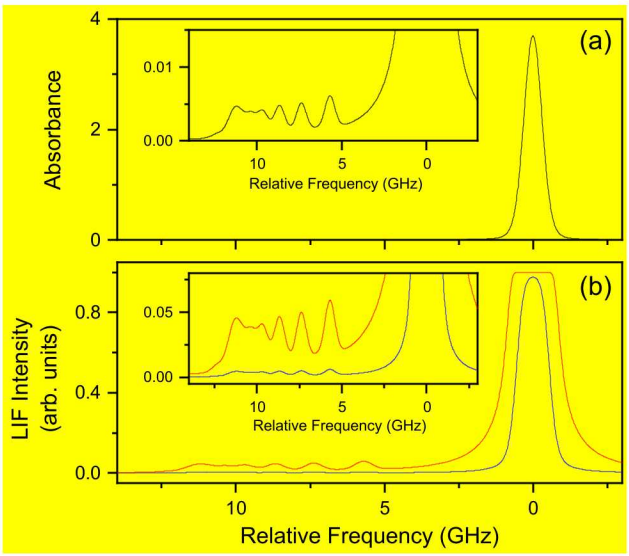

Figure 8. Simulated absorption and LIF spectra for U I 763.385 nm transition. (a) Absorbance spectrum with 0.7% ^{235}U. (b) LIF intensity spectrum calculated from the absorbance spectrum (blue, lower) and 10× absorbance spectrum (red, upper). Insets have re-scaled y-axis to show ^{235}U hyperfine structure.

High analytical accuracy for laboratory methods is typically achieved by performing calibration to known standards. The isotope ratio determined from the TRAS data at later times in the plasma is approaching the known isotope ratio for NU, which is encouraging for a preliminary measurement using this calibration-free technique. At this level of accuracy, it would be possible to distinguish depleted uranium (<0.3%), natural uranium (0.73%), and low-enriched uranium (~3-20%) [33]. The large difference in peak areas for enrichments near the extremes presents difficulties for measuring the major isotope peak accurately while at the same time measuring the minor isotope above the noise floor, and we expect that accuracy will improve significantly as isotope concentrations move towards balanced. As we refine our technique we expect to find lines that are better separated and will yield more accurate isotope ratios. We also believe that using a model fit to determine peak areas would improve the accuracy of the simple numerical integration used here. Model-fitting to the wings of the ^{238}U line was investigated here but the heavily absorbed ^{238}U lineshape, varying strongly in time, yielded inconsistent results, and additional work is needed.

4. Conclusions

In this study, isotopic shift and hyperfine structure analysis of selected U transitions in a laser-produced plasma were carried out using tunable optical spectroscopic tools such as LIF and LAS. The results showed that the isotopic shifts between ^{238}U and ^{235}U are entangled with hfs of ^{235}U. The time-integrated 2D-FS recorded using collinear pump-probe geometry showed plasma reabsorption effects. Time-resolved laser-absorption spectroscopy was carried out for evaluating the optical absorption and estimating the hyperfine constants. Our results highlight that the hfs constants for U can be empirically estimated through the use of model regressions applied to spectra generated in high-temperature and high-density laser-produced plasma systems. The measured isotope ratio exceeds the

expected value for that of NU at early times but approaches the expected value at later times of plasma evolution. The reabsorption effects seen in the LIF signal measurement is caused by the use of natural U metal target. The LIF calibration curves and the fluorescence phenomenon are inherently non-linear. LIF signal intensity typically is directly proportional to the absorbed energy. However, the absorbed energy is only linear with absorber number density at low concentrations. Previous studies highlighted that LIF is well-suited for trace detection down to ~a few ppm limit of detection (LOD) and in this regard the concentration of 0.7% of ^{235}U itself can be considered high for LIF experiments [36, 37]. It indicates that although the optical spectroscopy of laser ablation plumes is well suited for trace analysis, and the plasma reabsorption effects must be considered for quantification of isotopic ratio analysis in bulk samples. Hence the accuracy and analytical merits of the measurement can be significantly improved by using samples containing trace amounts of isotopes assisted by calibration (using multiple samples with known isotope ratios).

Funding: Office of Defense Nuclear Nonproliferation (DNN); National Nuclear Security Administration (NNSA); U.S. Department of Energy (DOE) (DE-AC05-76RL01830), and Sandia National Labs' Lab Directed Research and Development Office. This paper describes objective technical results and analysis. Any subjective views or opinions that might be expressed in the paper do not necessarily represent the views of the U.S. Department of Energy or the United States Government.

References

1. Harilal, S.S., et al., *Optical spectroscopy of laser-produced plasmas for standoff isotopic analysis.* Applied Physics Reviews, 2018. **5**(2): p. 021301.
2. Smith, C.A., et al., *Pu-239/Pu-240 isotope ratios determined using high resolution emission spectroscopy in a laser-induced plasma.* Spectrochim. Acta Part B, 2002(57): p. 929-937.
3. Cremers, D.A., et al., *Monitoring Uranium, Hydrogen, and Lithium and Their Isotopes Using a Compact Laser-Induced Breakdown Spctroscopy (LIBS) Probe and High-Resolution Spectrometer.* Applied Spectroscopy, 2012. **66**(3): p. 250-261.
4. Smith, B.W., et al., *Measurement of uranium isotope ratios in solid samples using laser ablation and diode laser-excited atomic fluorescence spectrometry.* Spectrochim. Acta Part B, 1999. **54**: p. 943-958.
5. Miyabe, M., et al., *Absorption spectroscopy of uranium plasma for remote isotope analysis of next-generation nuclear fuel.* Applied Physics a-Materials Science & Processing, 2013. **112**(1): p. 87-92.
6. Taylor, N.R. and M.C. Phillips, *Differential laser absorption spectroscopy of uranium in an atmospheric pressure laser-induced plasma.* Optics Letters, 2014. **39**(3): p. 594-597.
7. Phillips, M.C., et al., *Two-dimensional fluorescence spectroscopy of uranium isotopes in femtosecond laser ablation plumes.* Scientific Reports, 2017. **7**: p. 3784.
8. Miyabe, M., et al., *Laser ablation absorption spectroscopy for remote analysis of uranium.* Hyperfine Interactions, 2013. **216**(1-3): p. 71-77.
9. Hartig, K., et al., *Impact of oxygen chemistry on the emission and fluorescence spectroscopy of laser ablation.* Spectrochimica Acta Part B-Atomic Spectroscopy, 2017. **135**: p. 54-62.
10. Harilal, S.S., N.L. LaHaye, and M.C. Phillips, *High-Resolution Spectroscopy of Laser Ablation Plumes Using Laser-Induced Fluorescence.* Optics Express, 2017. **25** (3): p. 2312.
11. Goueguel, C., et al., *Resonant laser-induced breakdown spectroscopy for analysis of lead traces in copper alloys.* Journal of Analytical Atomic Spectrometry, 2011. **26**(12): p. 2452-2460.
12. Liu, L., et al., *Time-resolved resonance fluorescence spectroscopy for study of chemical reactions in laser-induced plasmas.* Optics Express, 2017. **25**(22): p. 27000-27007.
13. Nagli, L. and M. Gaft, *Combining Laser-Induced Breakdown Spectroscopy with Molecular Laser-Induced Fluorescence.* Applied Spectroscopy, 2016. **70**(4): p. 585-592.
14. Gao, P.Y., et al., *Determination of antimony in soil using laser-induced breakdown spectroscopy assisted with laser-induced fluorescence.* Applied Optics, 2018. **57**(30): p. 8942-8946.
15. Oba, M., et al., *Isotope shift and hyperfine structure of the highly excited atomic uranium.* Eur. Phys. J. D, 2002. **21**: p. 255-260.
16. Nielsen, U., et al., *^{235}U II hyperfine structures measured by collinear fast-beam-laser and radio-frequency-laser double-resonance spectroscopy.* J. Opt. Soc. Am. B, 1984. **1**: p. 284-292.
17. Demers, Y., et al., *Hyperfine structure measurements on some ^{235}U levels by laser fluorescence spectroscopy.* JOSA B, 1986. **3**: p. 1678-1680.
18. Böhm, H.-D.V., W. Michaelis, and C. Weitkamp, *Hyperfine Structure and Isotope Shift Measurements on ^{235}U and Laser Separation of Uranium Isotopes by Two-step photoionization.* Opt. Commun., 1978. **26**: p. 177 -182.
19. Miyabe, M., et al., *Laser ablation absorption spectroscopy for isotopic analysis of plutonium: Spectroscopic properties and analytical performance.* Spectrochim. Acta B, 2017. **134**: p. 42-51.
20. Bushaw, B.A. and N.C. Anheier, *Isotope ratio analysis on micron-sized particles in complex matrices by Laser Ablation-Absorption Ratio Spectrometry.* Spectrochimica Acta Part B-Atomic Spectroscopy, 2009. **64**(11-12): p. 1259-1265.
21. King, L.A., et al., *Rubidium isotope measurements in solid samples by laser ablation-laser atomic absorption spectroscopy.* Spectrochim. Acta Part B, 1999. **54**: p. 1771-1781.
22. Bergevin, J., et al., *Dual-Comb Spectroscopy of Laser-Induced Plasmas.* Nature Communications, 2018. **9**: p. 1273.
23. Harilal, S.S., N.L. LaHaye, and M.C. Phillips, *Two-dimensional fluorescence spectroscopy of laser-produced plasmas.* Optics Letters, 2016. **41**(15): p. 3547-3550.
24. Palmer, B.A., R.A. Keller, and J. R. Engleman, *An Atlas of Uranium Emission Intensities in a Hollow Cathode Discharge*, in 1980, Los Alamos Scientific Laboratory.
25. Avril, R., A. Ginibre, and A. Petit, *On the hyperfine structure in the configuration $5f^3 6d7s^2$ of neutral uranium.* Z. Phys. D 1994. **29**: p. 91-102.
26. Gangrsky, Y.P., et al., *Hyperfine anomaly in the f(3)ds(2) L-5(6)0, f(3)dsp M-7(7) and f(3)dsp L-7(6) levels in UI.* Zeitschrift Fur Physik D-Atoms Molecules and Clusters, 1997. **42**(1): p. 1-4.
27. Harilal, S.S., B.E. Brumfield, and M.C. Phillips, *Standoff analysis of laser-produced plasmas using laser-induced fluorescence.* Optics Letters, 2018. **43**(5): p. 1055-1058.
28. Chan, G.C.Y., et al., *Isotopic determination of uranium in soil by laser induced breakdown spectroscopy.* Spectrochimica Acta Part B-Atomic Spectroscopy, 2016. **122**: p. 31-39.
29. Yan, P., et al., *Measurements of hyperfine structure and isotope shift for atomic uranium by laser induced-fluorescence spectroscopy.* Chinese Journal of Lasers, 1992. **1**: p. 409.
30. Axner, O., et al., *Line strengths, A-factors and absorption cross-sections for fine structure lines in multiplets and hyperfine structure components in lines in atomic spectrometry - a user's guide.* Spectrochimica Acta Part B-Atomic Spectroscopy, 2004. **59**(1): p. 1-39.

31. Emery, G., *Hyperfine Structure*, in *Springer Handbook of Atomic, Molecular, and Optical Physics*, G. Drake, Editor. 2006, Springer New York: New York, NY. p. 253-260.
32. Childs, W.J., O. Poulsen, and L.S. Goodman, *High-precision measurement of the hyperfine structure of the 620-cm^{-1} metastable atomic level of ^{235}U by laser-rf double resonance.* Opt. Lett. , 1979. **4**: p. 63-65
33. *Live Chart of Nuclides: nuclear structure and decay data (https://www-nds.iaea.org/relnsd/vcharthtml/VChartHTML.html)*. Available from: https://www-nds.iaea.org/relnsd/vcharthtml/VChartHTML.html.
34. Burns, I.S. and C.F. Kaminski, *Diode Laser Induced Fluorescence for Gas-Phase Diagnostics.* Zeitschrift Fur Physikalische Chemie-International Journal of Research in Physical Chemistry & Chemical Physics, 2011. **225**(11-12): p. 1343-1366.
35. McManus, J.B., D.D. Nelson, and M.S. Zahniser, *Design and performance of a dual-laser instrument for multiple isotopologues of carbon dioxide and water.* Optics Express, 2015. **23**(5): p. 6569-6586.
36. Measures, R.M. and H.S. Kwong, *Tablaser - Trace (Element) Analyzer Based on Laser Ablation and Selectively Excited Radiation.* Applied Optics, 1979. **18**(3): p. 281-286.
37. Kwong, H.S. and R.M. Measures, *Trace-Element Laser Microanalyzer with Freedom from Chemical Matrix Effect.* Analytical Chemistry, 1979. **51**(3): p. 428-432.

Highlights:

- Absorption and fluorescence spectroscopy of U plasmas
- Isotopic shift and hyperfine structures analysis of U
- Estimation of HFS constants of selected U transitions
- Plasma reabsorption in cw-LIF measurements
- U isotopic ratio analysis

Graphical Abstract:

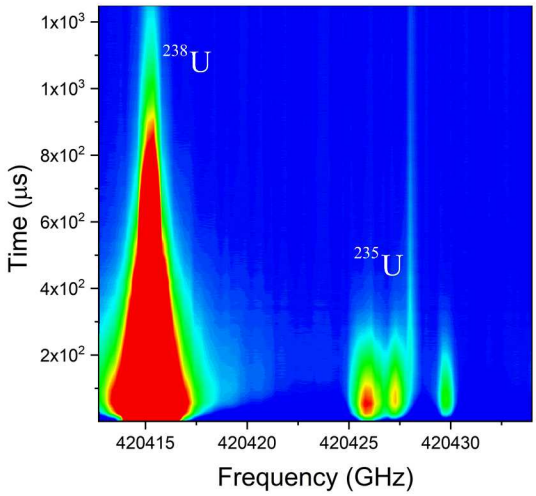

Dear Editor,

The authors thank the reviewers for their favorable reviews and constructive comments regarding our manuscript SAB_2020_25, "Hyperfine structures and isotopic shifts of uranium transitions using tunable laser spectroscopy of laser ablation plumes". We have addressed the concerns raised by the reviewers. Point by point replies to the reviewer's comments is listed below along with changes made in the revised text. We hope the present version of the manuscript is acceptable for publication in Spectrochimica Acta B.

Reviewer 1:

Line 106: please indicate that you analyze uranium metal. This precision is in the abstract but not in the text.

The revised test (experimental set up) reads "The target was a natural uranium metal,…"

Figures 2 and 3: the spectral range is < 40 pm, whereas the spectrometer resolution is 40 pm (line 130). Please mention explicitly that the plume emission is spectrally integrated.

We used a Czerny-Turner spectrograph with 2400 grooves/mm grating (spectral resolution ~ 40 pm) as a detector for analyzing the LIF signal. Please note that the spectral resolution of LIF is governed by the excitation laser linewidth (which is ≤100 kHz (≤ 0.2 fm) in the present experiment), and the line broadening mechanisms in the plasma. For clarity, the following sentences are added in the revised text.

The spectral resolution available for LIF measurement of the LPP system is governed by the linewidth of the excitation laser beam and the various line broadening mechanisms present in a laser-produced plasma system. Instead, the available spectral resolution for an emission spectroscopic instrumentation is dictated by the spectrograph resolution.

Fig. 2b: the modeled absorption spectrum is displayed as LIF intensity.

The authors thank the reviewer for pointing out this discrepancy. We removed the spectral simulation from Figure 2.

Fig. 7: the isotope ratio is always biased by different phenomena, whatever the delay. Perspectives are given concerning lines understudy and numerical aspects (lines 630-635). Any suggestion/discussion to improve analytical results from an instrumental point of view (pressure, the distance between the sample surface and the LAS probe beam, ablation fluence...)?

The reviewer is correctly pointing out the complexity of a laser-produced plasma system and the parametric space available for improving the analytical results. In the present experiment, we used a U bulk metal target (100% U). The analytical merits can be significantly improved with the use of a low-concentration sample assisted by calibration. This description is provided in the conclusion section.

Similarly to LAS, why didn't authors do time-resolved LIF in order to avoid optical saturation? With their ICCD it could have been possible.

We made time-resolved LIF experiments using the present experiment. However, signal to noise ratios using smaller gate widths were found to be not good.

-Reviewer 2

We thank the reviewer for the favorable overall response along with highlighting a significant problem in the discussion section about the optical saturation effects. The reviewer is correct that the authors used the word optical saturation effects inappropriately and we apologize for generating confusion in this regard. Point by point reply to reviewer's comments is given below with clarifications and changes in the text.

1) I would like to know the laser energy (rather than having to back-calculate from fluence and the spot size at the sample.

We used 48 mJ laser pulse energy for producing plasmas. These details are added in the revised text.

2) I would appreciate knowing what kind of prism was used to select against plasma emission in the LAS experiments (e.g. equilateral?), though this is a minor issue.

   We used a 1" right-angled prism for spectral filtering. The revised text is modified to include these details.

3) More importantly, the authors describe the fiber-optic collection as spatially-integrated in their LIF measurements. This depends on the fiber and the optic(s) (if any) used to direct light into the fiber- in some cases, the measurement could be considered simply "line-of-sight" (as opposed to "spatially integrated"), depending on the optics. Many of us use imaging with NA-matching onto the fiber face explicitly to generate spatially resolved measurements. I bring this up because there could still be prefilter effects (never mentioned with this name, though the authors do mention "opacity effects", which could be prefilter effects or postfilter effects in my understanding), depending on the geometric relationship between the excitation and collection volumes. The relative relation of excitation and collection volumes could also be important for Postfilter effects (I believe the authors allude to these, though not by this name?). I bring this all up because the explanation that the authors give for the isotope ratio mismatch is not satisfying and they should consider other effects.

The authors thank the reviewer for bringing this interesting question. We used a fiber optic assembly employing a plano-convex lens (LF22U50, focal length = 5cm, aperture 22mm) for collecting the LIF signal from the plasma. The light collection assembly was positioned ~ 10 cm and at near-normal angle to the plasma expansion direction. We used a He-Ne laser beam (coupled to the fiber) for evaluating the area of light collection. Using this method, we made sure that the measurement was spatially-integrated. The size of the LIF laser for exciting the plasma was ~ 4mm. The LIF excitation beam was also operated at near-normal angle with respect to target and overfilling the plasma. We agree with the reviewer that the angle of incidence of the excitation beam as well as the collection angle will indeed affect the measurement and could contribute isotopic mismatch. Ideally, it is better to excite the plasma at a certain location (similar to LAS). However, our aim was to evaluate the LIF excitation in a standoff configuration where collinear excitation is a prerequisite.

4) Presumably, the sample is natural uranium metal? The authors never mention this. Also, in line 48 of p. 7, the authors suggest that we should be impressed by seeing 0.7% 235U in the plasma with such good signal to noise. 0.7% is an extremely high concentration by LA-LIF standards. Singly ppm LODs are possible in many cases. In fact, this brings up another important consideration in LIF that the authors do not seem to address: LIF calibration curves and the fluorescence phenomenon are inherently non-linear. LIF is directly proportional to the absorbed energy (in the volume imaged by the detection optics, but I dealt with that issue above). The absorbed energy, on the other hand, **is only linear with absorber number density**

at low concentrations… absorbance (-logI/Io) is linear with concentration forever so long as the absorbers do not perturb each other through collisions. Fluorescence is directly proportional to the absorbed energy, not absorbance. Fluorescence measurements are only linear because they are typically made at (vanishingly) low concentrations, where the absorbance is linear (as usual) and the amount of absorbed energy can be approximated as linear (i.e. the higher order terms of the Taylor expansion can be neglected). This is not an "opacity" effect but rather a fundamental mathematical consideration in fluorescence spectroscopy. The authors likely know this better than I, but they do not bring up this inherent nonlinearity in their discussion; fluorescence has a limited LDR due to this math and this is going to be a problem for measuring isotope ratios far from 50:50 unless the absorbances of both isotopes are so vanishingly small that the higher-order terms of the Taylor expansion can be ignored. This must be incorporated into the discussion.

We agree with the reviewer's suggestion that LIF is best suited for trace element analysis. The use of bulk element for LIF of LA may lead to deviation in the isotopic analysis. We also apologies for not specifically mentioning the use of U natural metal target for the present study.

We added a detailed discussion about this topic in the revised text (please check the reply for suggestion 5)

5) What follows is my primary issue with the paper. The authors repeatedly suggest that their measurements, both absorption and fluorescence, deviate from expected peak ratios due to "optical saturation effects." In my understanding, optical saturation effects in laser absorption and fluorescence spectroscopy are due to stimulated absorption (resulting from some combination of high absorption oscillator strength and high excitation laser spectral irradiance) outstripping all other processes repopulating the lower state of the transition and depopulating the upper state of the transition. As a result, the upper state population builds to the point that stimulated absorption is matched by stimulated emission and no further absorption is possible. The authors repeatedly cite these "optical saturation effects" as the source of their errors. This is easily checked for- simply lower your excitation laser power. This is such a simple and obvious check, it should have been done as part of the experiments. Thus, the authors either need to stop citing "optical saturation effects" and consider the other sources of nonlinearity or make this experiment. I think that the authors imply that "saturation effects" occur with 238U more than 235U. This is not the case. Prefilter and postfilter effects would be greater with the more concentrated absorber, though. In the event that prefilter effects are causing nonlinearity (specifically sublinearity) of the fluorescence signal, decreasing the excitation intensity will actually increase the disparity between measured and expected peak ratios in some cases. When the transition is fully saturated along the whole length of the viewed plasma-laser interaction volume, the upper state number density becomes constant (simply a ratio of the upper and lower state degeneracies) and the prefilter effect (and the related issue of fluorescence's linearity being inherently an approximation) decreases, eventually becoming negligible. In either case, the source of fluorescence nonlinearity can be diagnosed by changing the excitation laser power.

The authors really must either perform this diagnostic or generally speculating about "optical saturation effects." Without this information on the sublinearity, the paper (in its current state) is lessened, since the only novelty is the hyperfine information. The paper should be improved both by performing the relatively simple experiments to rule out different sources and generally in the discussion of the sources of nonlinearity (consider prefilter, postfilter, inherent nonlinearity, etc. and use more precise terminology).

As a final aside, even absorbance can appear "sublinear" at high absorbances due to uncorrected dark signals and the wings of the laser emission line, despite the exquisite fwhm or due to beam steering because of the high gradients in refractive index at the absorption line. Of course, this is only the apparent absorbance that is nonlinear- the authors know all this, no doubt, but do not reference it, oversimplifying their discussion.

The authors generally underrepresent the complexity of their experiments- their interpretation of the data is inadequate. As a result, I recommend rejection with the understanding that the experiments are not fundamentally flawed and require a relatively straightforward improvement, with improvement to the discussion also necessary.

The authors thank the reviewer for highlighting this issue. The reviewer is correct that the authors used the word "optical saturation effects" inappropriately in explaining the isotopic ratio discrepancy seen in the measurement. This is a confusing aspect of the article. We previously noticed that the temporal decay of LIF emission for bulk and trace species was different and it changes with laser energy (ablation efficiency). However, our results showed that the LIF signal changed approximately linear with excitation laser power. Please note that we kept the beam size ~4 mm for overfilling the plasma for avoiding power broadening.

We added the following details in the revised paper to address review

The LIF emission signal is generated from the energy absorbed from the LIF excitation laser. Based on Eqn. (3) in Ref. (Burns & Kaminski, 2011), the detected LIF signal $S_F(\lambda_{ex}, t)$ can be expressed in a simplified form as:

$$S_F(\lambda_{ex}, t) = S_0 \cdot I_0 \cdot \left[1 - e^{-A(\lambda_{ex}, t)}\right] \qquad \text{Eqn. (4)}$$

where λ_{ex} is the wavelength of the laser exciting the LIF transition, t is time, S_0 is a constant factor incorporating collection area/efficiency and fluorescence quantum yield, I_0 is the incident laser intensity, and $A(\lambda_{ex}, t)$ is the absorbance experienced by the laser. For a simplified case of a spatially-uniform plasma with length L, the absorbance is given by $A(\lambda_{ex}, t) = \sigma_{12}(\lambda_{ex}) \cdot N_1(t) \cdot L$, where $\sigma_{12}(\lambda_{ex})$ is the absorption cross-section, $N_1(t)$ is the atomic population in the lower state pumped by the LIF excitation laser. Eqn. (4) is linear in the incident laser intensity I_0 and thus ignores optical saturation or optical pumping effects arising at high laser intensities, which is more common with pulsed LIF than with the CW LIF used in our experiments. Eqn. (1) also ignores any reabsorption of the LIF emission. For $A(\lambda_{ex}, t) \ll 1$, Eqn. (1) simplifies to $S_F(\lambda_{ex}, t) \sim S_0 \cdot I_0 \cdot [\sigma_{12}(\lambda_{ex}) \cdot N_1(t) \cdot L]$ and under these conditions of low optical density the LIF signal is linear with atomic number density. Under conditions of very high optical density $A(\lambda_{ex}, t) \gg 1$, Eqn. (4) approaches a constant value $S_F(\lambda_{ex}, t) \sim S_0 \cdot I_0$ corresponding to complete absorption of the incident laser after which the LIF signal cannot increase further. Thus, under conditions of high optical density, the LIF intensity is nonlinear with the atomic number density and approaches a maximum value. Correspondingly, because the absorbance depends on the excitation wavelength, the lineshape of the LIF excitation spectrum deviates from the absorbance spectrum lineshape $\sigma_{12}(\lambda_{ex})$.

The results in Fig. 4 verify that the 235U absorbance is low (<0.03) throughout the plasma evolution. Thus, it is reasonable to assume the LIF excitation spectra are linear in 235U number density and the LIF excitation spectra are proportional to the absorbance spectra. In contrast, the 238U absorbance is high (>0.1 most times and >1 in many cases) near the line center which leads to the distorted LIF excitation spectra observed in Fig. 2 and Fig. 3. It is also noted that the absorbance spectrum may also become distorted in the presence of high optical density, leading to nonlinearity between the area under the absorbance peak and the atomic number density. Besides, it can be difficult to measure high absorbances accurately given the high dynamic range required to measure both the low transmitted light and the high incident intensity.

Figure 7(a) and Fig. 8(a) show simulated absorbance spectra for the U I 713.087 nm and the U I 763.385 nm transitions, respectively, including the modeled hyperfine structure. Individual peaks were modeled by Voigt profiles with 660 MHz Gaussian FWHM and 100 MHz Lorentzian FWHM. The areas of the ^{235}U and ^{238}U peaks are scaled to represent natural U with 0.73% ^{235}U. In absorbance, the peak areas are assumed to be linear with atomic number density over the range plotted. Figure 7(b) and Fig. 8(b) show simulated LIF excitation spectra modeled using Eqn. (1) based on the absorbance spectra shown in Fig. 7(a) and Fig. 8(a), respectively. The lower blue curves show the modeled LIF signal for the absorbance as plotted in (a), and the upper red curves show the modeled LIF signal with the absorbance spectra multiplied by 10. The high absorbance near the ^{238}U peaks leads to a highly nonlinear dependence of LIF emission intensity on absorbance. The net effect of the nonlinearity is an apparent increase in height of the ^{235}U peaks relative to the ^{238}U peaks in the LIF excitation spectrum. Qualitatively similar effects on the relative peak areas of ^{235}U and ^{238}U were observed in Fig. 2 and Fig. 3, which we attribute primarily to the high absorbance of the ^{238}U peak, as verified by the TRAS results shown in Fig. 4. Besides, other nonlinearities in the LIF emission signal due to optical saturation or reabsorption of emitted light may be present, leading to additional deviations of peak shapes and/or relative heights of ^{235}U versus ^{238}U peaks measured in the experimental LIF spectra.
In general, while LIF provides high sensitivity for trace element detection, it is challenging to use LIF for quantitative measurements of bulk elements due to the inherent nonlinearity of LIF signal with atomic number density under conditions of high absorbance. The same challenges exist for isotope ratio measurements when the isotopic abundances differ by large amounts. Possible solutions to improve quantification of isotope ratios using LIF include measuring different lines for major and minor isotopes to equalize the absorbance, although temperature-dependence of the line strengths must also be considered. Similar approaches are used with laser absorption spectroscopy for the detection of molecular isotopologues (McManus, Nelson, & Zahniser, 2015).

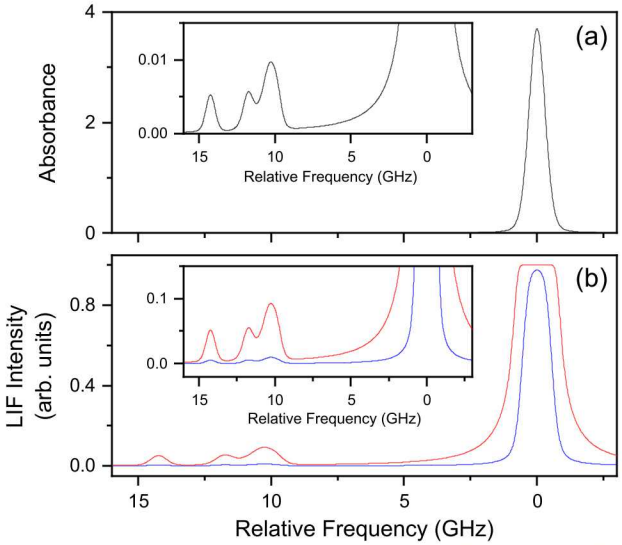

Figure 7. Simulated absorption and LIF spectra for U I 713.087 nm transition. (a) Absorbance spectrum with 0.7% ^{235}U. (b) LIF intensity spectrum calculated from absorbance spectrum (blue, lower) and 10× absorbance spectrum (red, upper). Insets have re-scaled y-axis to show ^{235}U hyperfine structure.

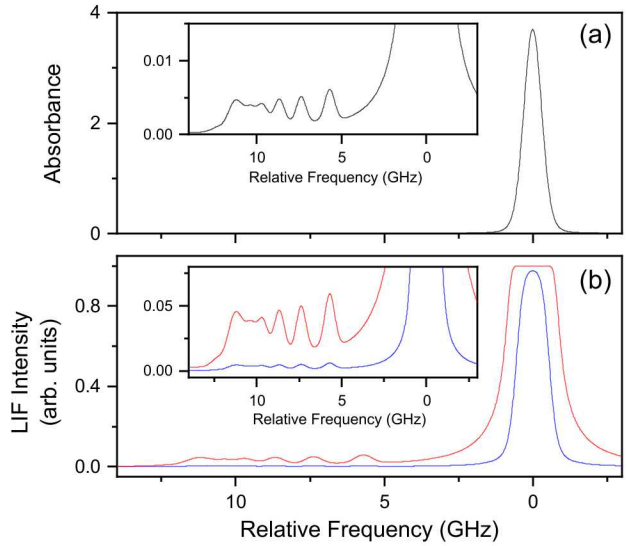

Figure 8. Simulated absorption and LIF spectra for U I 763.385 nm transition. (a) Absorbance spectrum with 0.7% ^{235}U. (b) LIF intensity spectrum calculated from absorbance spectrum (blue, lower) and 10× absorbance spectrum (red, upper). Insets have re-scaled y-axis to show ^{235}U hyperfine structure.

Burns, I. S., & Kaminski, C. F. (2011). Diode Laser Induced Fluorescence for Gas-Phase Diagnostics. *Zeitschrift Fur Physikalische Chemie-International Journal of Research in Physical Chemistry & Chemical Physics, 225*(11-12), 1343-1366. doi:10.1524/zpch.2011.0182

McManus, J. B., Nelson, D. D., & Zahniser, M. S. (2015). Design and performance of a dual-laser instrument for multiple isotopologues of carbon dioxide and water. *Optics Express, 23*(5), 6569-6586. doi:10.1364/oe.23.006569